



## Effects of unique band structure of $h$ -BN probed by photocurrent excitation spectroscopy

Samuel J. Grenadier, Avisek Maity, Jing Li, Jingyu Lin\*, and Hongxing Jiang\*

Department of Electrical and Computer Engineering, Texas Tech University, Lubbock, TX 79409, United States of America

\*E-mail: [jingyu.lin@ttu.edu](mailto:jingyu.lin@ttu.edu); [hx.jiang@ttu.edu](mailto:hx.jiang@ttu.edu)

Received April 13, 2022; revised April 22, 2022; accepted April 28, 2022; published online May 13, 2022

By employing a photocurrent excitation spectroscopy measurement, a direct bandgap of  $\sim 6.46$  eV has been resolved for the first time in thick B-10 enriched  $h$ -BN films. Together with previous band calculations, an unconventional energy diagram has been constructed to capture the unique features of  $h$ -BN:  $h$ -BN has a minimum direct bandgap of  $\sim 6.5$  eV and a bandgap of  $\sim 6.1$  eV which is indirect with the conduction band minimum (CBM) at M-point and valence band maximum (VBM) at K-point in the Brillouin zone, and the energy levels of the donor and acceptor impurities are measured relative to CBM and VBM, respectively. © 2022 The Japan Society of Applied Physics

**A**s an ultrawide bandgap semiconductor, hexagonal boron nitride ( $h$ -BN) is considered one of the last frontiers of semiconductors.<sup>1–3)</sup> Much progress has been achieved over the last decade with worldwide research efforts, from bulk crystal and epilayer growth, fundamental band structure and basic properties understanding, to device applications. However, many questions, some of which are considered very fundamental, remain ambiguous and need to be further understood.

While optical absorption studies often suggest a direct bandgap gap of around 6.0–6.1 eV for  $h$ -BN,<sup>4–6)</sup> theoretical<sup>7,8)</sup> and two-photon spectroscopy studies<sup>9)</sup> provided strong evidence that  $h$ -BN has an indirect bandgap of around 6.0–6.1 eV with the conduction band minimum (CBM) and valence band maximum (VBM) located at M- and K-point in the Brillouin zone (BZ), respectively. On the other hand, photoluminescence (PL) emission spectroscopy involving excitonic transitions together with exciton binding energy measurements, donor-acceptor pair transitions and photocurrent excitation spectroscopy studies often reveal an energy bandgap around 6.4–6.5 eV.<sup>3,10–14)</sup> There has been no clear explanation to account for this ambiguity so far. Moreover, a simple and clear picture for describing the impurity energy levels in such an ultrawide but indirect bandgap material is still lacking. The present work tries to address these fundamental questions. Understanding the rich physical properties of  $h$ -BN will support further advancement of the material and device technologies based on this important member of the III-nitride wide bandgap semiconductor family.

One of the distinctive applications which sets  $h$ -BN apart from traditional III-nitrides is its promising applications for thermal neutron detection<sup>14–17)</sup> owing to the large nuclear interaction cross section between the element of B-10 ( $^{10}\text{B}$ ) and thermal neutrons of 3840 barn,<sup>18)</sup> which yields an absorption length of thermal neutrons in 100%  $^{10}\text{B}$  enriched  $h$ -BN ( $h$ - $^{10}\text{BN}$ ) of 47  $\mu\text{m}$ .<sup>15,16)</sup> As such,  $h$ - $^{10}\text{BN}$  neutron detectors require a large thickness in order to provide an adequate intrinsic detection efficiency. More recently, thick layers of freestanding  $h$ - $^{10}\text{BN}$  wafers have been produced<sup>14–17)</sup> and  $h$ - $^{10}\text{BN}$  thermal neutron detectors with a record high detection efficiency of 59% and sensitivity among solid-state neutron detectors have been realized.<sup>16)</sup> Due to the requirements of large thicknesses and high growth temperatures,  $h$ - $^{10}\text{BN}$  materials used for thermal neutron detector fabrication tend to contain many impurities and defects. It was speculated that oxygen and its related defects

are the dominant impurities that limit the charge collection efficiency of  $h$ - $^{10}\text{BN}$  neutron detectors.<sup>14,16)</sup> The oxygen impurities were diffused from sapphire substrate due to the combination of relatively high growth temperatures and long growth times employed during epilayer growth.<sup>14,16)</sup> Furthermore, there was also strong evidence that the presence of these defects is a major obstacle that limits the charge collection efficiency in  $h$ - $^{10}\text{BN}$  neutron detectors.<sup>14–16)</sup> Thus, obtaining an improved understanding of the basic properties of these impurities/defects, including their physical nature and energy levels, will also provide useful insights to guide material growth and to further advance the boron nitride neutron detector technologies.

The sample used in this study is similar to those used for the construction of thermal neutron detectors.<sup>14–17)</sup> A  $h$ - $^{10}\text{BN}$  wafer of about 100  $\mu\text{m}$  in thickness was grown by metal organic chemical vapor deposition on  $c$ -plane sapphire substrate at a temperature of  $\sim 1500$  °C. Freestanding  $h$ - $^{10}\text{BN}$  wafer was then obtained via self-separation during cooling down after epi-growth, owing to the layer structured  $h$ -BN which has a different thermal expansion coefficient than sapphire substrate, as schematically illustrated in Fig. 1(a). Photo of a freestanding  $h$ - $^{10}\text{BN}$  ¼-wafer (4-inches in diameter) is depicted in Fig. 1(b). The wafer was then cut into the desired shape by laser dicing for device fabrication and measurements. For photocurrent excitation spectroscopy measurements, a detector strip in the lateral geometry was fabricated. A highly resistive adhesive material (polyimide) was used to mount the detector strip on an insulating submount (sapphire). Metal contacts consisting of a bi-layer of Ni (100 nm)/Au (40 nm) were deposited on the two edges of the  $h$ - $^{10}\text{BN}$  strip using e-beam evaporation via a mask leaving  $\sim 100$   $\mu\text{m}$  of metal overlapping on the edges. Wire bonding was then performed to create an electrical connection between the deposited metal contacts and the bonding pads of a semiconductor device package. A micrograph of a finished device with a width of 2 mm is shown in Fig. 1(c) and a more detailed schematic illustration of the detector setup for the photocurrent excitation spectroscopy measurements is shown in Fig. 2(a). A broad light source covering a wavelength range between 170 and 2100 nm [model E-99 laser-driven light source by Energytiq] coupled with a triple grating monochromator was used as a variable wavelength excitation source with a spectral resolution of  $\sim 0.2$  nm. A source meter was used to apply voltages and an electrometer was used to record the photocurrents.

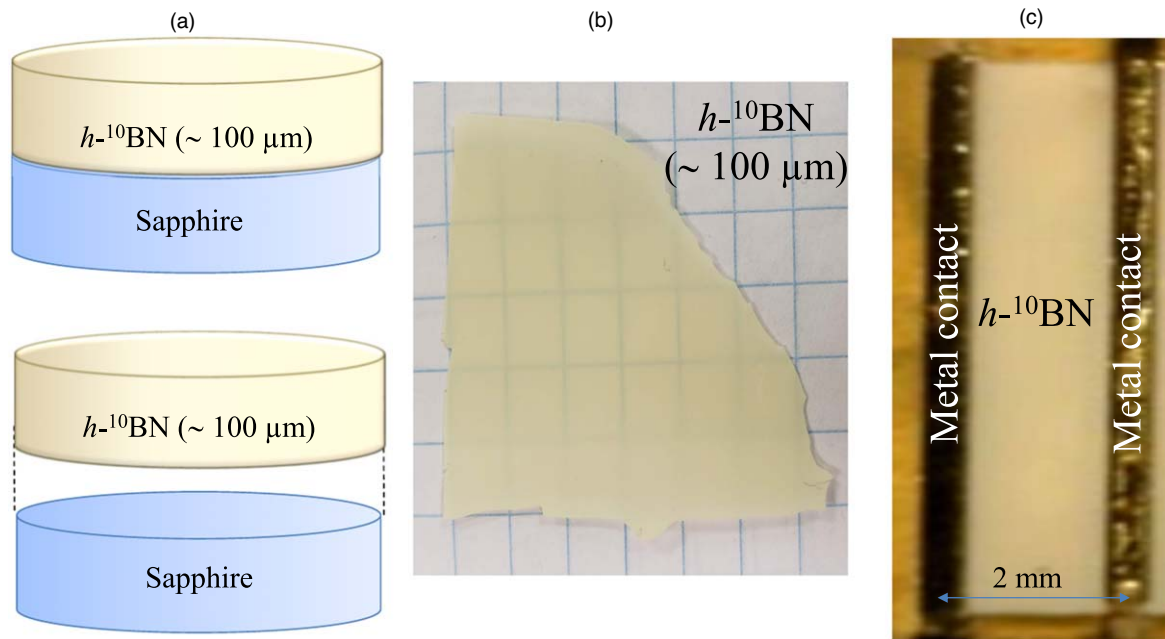


**Fig. 1.** (Color online) (a) A schematic diagram of freestanding  $h$ - $^{10}\text{BN}$  formation. (b) An optical image of a freestanding  $h$ - $^{10}\text{BN}$  wafer of  $\sim 100 \mu\text{m}$  in thickness. (c) An optical image of a fabricated  $h$ - $^{10}\text{BN}$  detector strip of 2 mm in width for photocurrent excitation spectroscopy measurements.

A recent theoretical study revealed that oxygen impurities tend to occupy the nitrogen sites,  $\text{O}_\text{N}$ , and act as donors located at about 0.61 eV below the conduction band.<sup>19</sup> Furthermore, the presence of  $\text{O}_\text{N}$  donors tends to shift the Fermi level toward the conduction band edge and reduces the formation energies of boron vacancies ( $\text{V}_\text{B}$ )-hydrogen complexes ( $\text{V}_\text{B}-\text{H}/\text{V}_\text{B}-2\text{H}$ ), which are acceptor-like deep level defects located at 1.65/1.54 eV above the valence band.<sup>19</sup> The determination of the energy levels of these impurities have been attempted previously in a similar  $h$ - $^{10}\text{BN}$  sample via measurements of photocurrent excitation spectra of electron and hole transport separately.<sup>20</sup> The measured photocurrent excitation spectrum for the hole transport exhibited a threshold energy at about  $\sim 5.9$  eV, whereas that for the electron transport exhibited a threshold energy at about  $\sim 4.9$  eV (shown in Fig. 22 of Ref. 20). The results suggested a donor level associated with  $\text{O}_\text{N}$  located at  $\sim 5.9$  eV above the valence band edge and an acceptor level related to  $\text{V}_\text{B}-\text{H}/\text{V}_\text{B}-2\text{H}$  located  $\sim 4.9$  eV below the conduction band edge. However, the bandgap value was left open.<sup>20</sup>

The minimum direct energy bandgap,  $E^{\text{dir}g}$ , can also be measured by utilizing the photocurrent excitation spectroscopy technique. In such a measurement, charge carriers are excited at the same k-point in the Brillouin zone followed by an immediate collection by the electrodes without involving relaxation to other band minimum or maximum points in the Brillouin zone. Therefore, a photocurrent excitation spectrum can resolve a spectral peak corresponding to the bandgap at the same k-point in the Brillouin zone, i.e. a direct energy bandgap. As illustrated in Fig. 2(a), in this configuration, by illuminating the entire surface of the sample the measured photocurrent is contributed by both the free electron and free hole conduction. The photocurrent excitation spectrum shown in Fig. 2(b) exhibits a dominant transition peak near 6.46 eV, for which we assign it to the band-to-band excitation involving the minimum direct bandgap,  $E^{\text{dir}g}$ , in  $h$ -BN. Since the photocurrent excitation spectrum can only record

photoexcited free electrons and holes at the same k-point in the Brillouin zone, the transition peaks corresponding to the photoexcitation across the indirect bandgap ( $E_g$ ) involving different k-points in the Brillouin zone can be excluded. The observation of spectral peaks corresponding to the free-exciton excitation is not expected from these thick films because of the presence of undesired impurities/defects. Additionally, the applied electric field is too weak to break up the excitons due to the large binding energy of excitons of  $\sim 700$  meV in  $h$ -BN.<sup>1-3,7,10</sup> The observed peak position at 6.46 eV corresponds well with previously observed direct bandgap values from photocurrent excitation spectra of bulk crystals<sup>12</sup> and thin films (30 nm in thickness)<sup>15</sup> of natural  $h$ -BN. Furthermore, the measured value agrees very well with a previous ab initio band structure calculation study which revealed a minimum direct bandgap of about 6.47 eV and the unique feature of the flatness of the M-K sector of the Brillouin zone in  $h$ -BN.<sup>6</sup> Although a more recent calculation based on  $GW$  approximation deviates slightly from the measured value, but also revealed a similar trend with a minimum direct bandgap across the entire flat M-K sector ranging from 6.54 to 6.7 eV in  $h$ -BN.<sup>7</sup> The flatness feature of the M-K sector also explains the observed high photocurrent near 6.46 eV since all the states crossing the entire M-K sector can be excited by the photons in this spectral range as well as the observation of intense exciton emissions in high-quality bulk crystals and thin films of natural  $h$ -BN.<sup>3,10,11</sup> The excellent agreement among the experimentally measured minimum direct bandgap values from  $h$ - $^{10}\text{BN}$  thick layers here, bulk crystals<sup>12</sup> and thin films (30 nm in thickness)<sup>15</sup> of natural  $h$ -BN and the theoretically calculated minimum direct bandgap values<sup>6,7</sup> implies that isotope has a negligible effect on the band structure of  $h$ -BN, as expected.

The observed minimum direct bandgap value of 6.46 eV in Fig. 2 and the threshold energy for a donor level at  $\sim 5.9$  eV above the valence band edge<sup>20</sup> provide an energy level of the presumed  $\text{O}_\text{N}$  donors to be  $E_\text{D}(\text{O}_\text{N}) = 6.46 - 5.9 = 0.56$  eV.

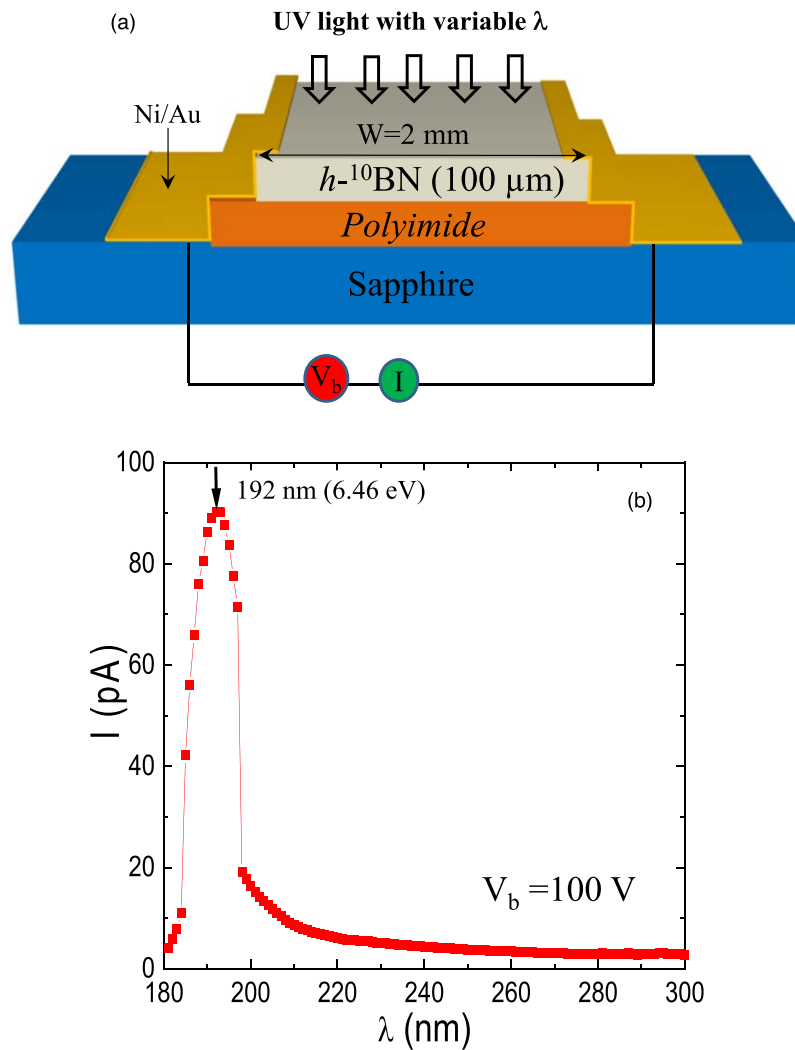


**Fig. 2.** (Color online) (a) The schematic setup for the photocurrent excitation spectroscopy measurement. The  $h$ - $^{10}\text{BN}$  detector strip used for the measurement is shown in Fig. 1(c). Two metal electrodes consisting of a bi-layer of Ni (100 nm)/Au (40 nm) were deposited on the two edges of the  $h$ - $^{10}\text{BN}$  strip using e-beam evaporation via a mask leaving  $\sim 100\ \mu\text{m}$  of metal overlapping on the edges. A highly resistive adhesive material (Polyimide) was used to mount the detector strip on an insulating sub-mount (sapphire). (b) Room temperature photocurrent excitation spectrum of a freestanding  $h$ - $^{10}\text{BN}$  sample with the entire sample surface under illumination by a variable wavelength excitation source.

Furthermore, the measured minimum direct bandgap in Fig. 2 together with the observed threshold energy for an acceptor level located at  $\sim 4.9\ \text{eV}$  below the conduction band edge<sup>20)</sup> also infers the energy level of the assumed  $(\text{V}_\text{B}-\text{H})/(\text{V}_\text{B}-2\text{H})$  complex deep acceptors to be  $E_\text{A}(\text{V}_\text{B}-\text{H}) = 6.46 - 4.9\ \text{eV} = 1.56\ \text{eV}$ . These measured values are in close agreement with the calculated values of  $E_\text{D}(\text{O}_\text{N}) \sim 0.61\ \text{eV}$  and  $E_\text{A}(\text{V}_\text{B}-\text{H}) \sim 1.65\ \text{eV}$  and  $E_\text{A}(\text{V}_\text{B}-2\text{H}) \sim 1.54\ \text{eV}$ .<sup>19)</sup> The agreement between the measured and calculated energy levels further supports the interpretation that  $\text{O}_\text{N}$  and  $(\text{V}_\text{B}-\text{H})/(\text{V}_\text{B}-2\text{H})$  are the dominant defects in these thick  $h$ -BN films. Since the diffusion of oxygen impurities from sapphire substrate is being identified as the primary cause of the presence of  $\text{O}_\text{N}$  and  $(\text{V}_\text{B}-\text{H})/(\text{V}_\text{B}-2\text{H})$  in thick  $h$ -BN films, it is then feasible to eliminate these defects via growth techniques developed for III-nitrides, including multiple buffer layers or dislocation filter layers for protecting as well as for improving the performance of top active layers.<sup>21–23)</sup>

Based on the experimentally measured minimum direct bandgap and energy levels of  $\text{O}_\text{N}$  and  $(\text{V}_\text{B}-\text{H})/(\text{V}_\text{B}-2\text{H})$  impurities together with the band structure calculations,<sup>7,8)</sup> a modified energy diagram can be constructed to provide a more straightforward understanding of the band structure

near the band edges and energy levels of the dominant impurities and defects in thick layers of  $h$ -BN. Figure 3(a) shows a standard way for describing the energy diagram near the band edges and impurity levels in semiconductors. We would like to point out that this standard energy diagram misses several important aspects of  $h$ -BN, such as the locations of CBM and VBM in  $k$ -space, minimum direct energy bandgap, and energy levels involved for direct photoexcitation of impurities and bands. Due to its ultrawide and indirect bandgap as well as the small difference between its direct and indirect energy bandgaps, we suggest a modified energy diagram as shown in Fig. 3(b). This modified energy diagram captures unique features of  $h$ -BN in comparison with other III-nitrides: (a) CBM and VBM are, respectively, indicated at the M- and K-points in the Brillouin zone, (b) donor energy levels are measured with respect to the CBM at the M-point, (c) acceptor energy levels are measured with respect to the VBM at the K-point, (d) other than the energy bandgap around  $E_\text{g} \approx 6.1\ \text{eV}$  with CBM and VBM located around M-point and K-point, respectively,<sup>7,8)</sup> the modified energy diagram of Fig. 3(b) also clearly reveals a minimum direct energy bandgap of  $E_\text{g}^\text{dir} \approx 6.5\ \text{eV}$ . Due to

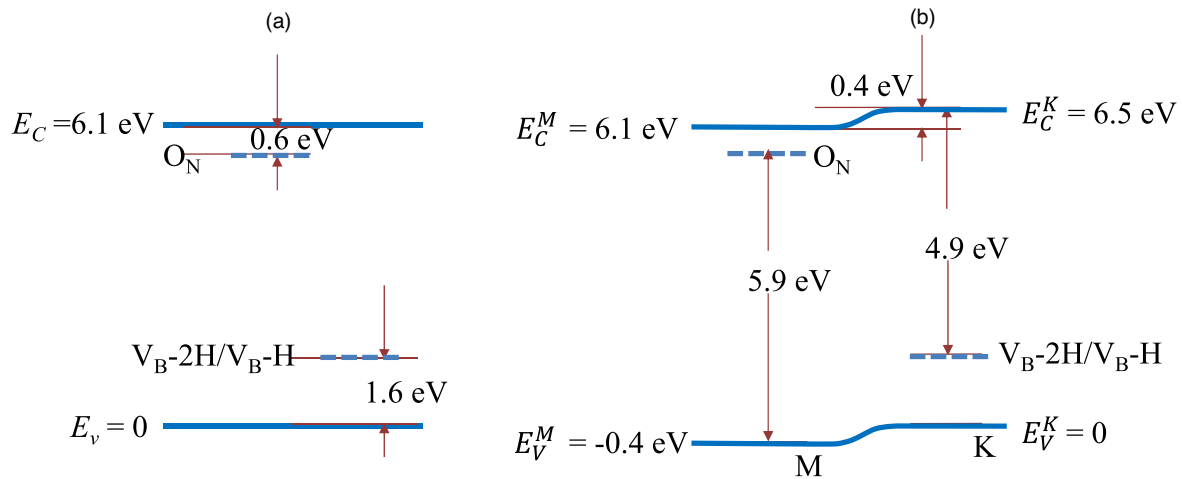


**Fig. 3.** (Color online) (a) A standard description of the energy band diagram of *h*-BN including the energy levels of the dominant impurities of  $O_N$  donors and  $V_B$ -H acceptors with an energy bandgap of  $\sim 6.1$  eV. (b) Proposed energy diagram including the energy levels of the dominant impurities of  $O_N$  donors and  $V_B$ -H acceptors to reflect the nature of indirect energy bandgap with the conduction band minimum (CBM) and the valence band maximum (VBM) located at M- and K-point, respectively, as well as the effect of a minimum direct bandgap in *h*-BN.

the flatness of the M–K sector of the Brillouin zone, the direct energy gap near M-point is very close to that near K-point, which means that the minimum direct energy bandgap is located either at M- or K-point in the Brillouin zone. We believe that the energy diagram of Fig. 3(b) provides a simpler picture to understand the energy levels involving photoexcitation of both donors and acceptors as well as the conduction and valence band edges. This analysis also indicates that the energy difference between the CBM at the M- and K-points as well as between VBM at the M- and K-points are around 0.4 eV. Such an effect is negligibly small in other indirect semiconductors such as Si. However, this effect becomes significant in *h*-BN due to its ultrawide bandgap.

In summary, photocurrent excitation spectroscopy has been employed to probe the minimum direct energy bandgap and energy levels of the dominant impurities/defects in thick  $h$ - $^{10}$ BN films. Experimental results together with previous band structure calculation studies put forward an unconventional energy diagram to provide a more straightforward understanding of the impurities energy levels and band structure involving CBM and VBM in *h*-BN. The identification of relevant energy levels, characteristics and origins of the dominant defects in *h*-BN are expected to guide the epitaxial growth processes to minimize the concentrations of the dominant defects and thereby help to further advance the *h*-BN material and device technologies.

**Acknowledgments** The research is supported by DOE ARPA-E (grant #DE-AR0001257). H. J. and J. L. are grateful to the AT&T Foundation for the support of Ed Whitacre and Linda Whitacre endowed chairs. The data that support the findings of this study are available within this manuscript.

- 1) Y. Kubota, K. Watanabe, O. Tsuda, and T. Taniguchi, *Science* **317**, 932 (2007).
- 2) K. Watanabe, T. Taniguchi, T. Niiyama, K. Miya, and M. Taniguchi, *Nat. Photonics* **3**, 591 (2009).
- 3) K. Watanabe, T. Taniguchi, and H. Kanda, *Nat. Mater.* **3**, 404 (2004).
- 4) T. Sugino, K. Tanioka, S. Kawasaki, and J. Shirafuji, *Jpn. Appl. Phys.* **36**, L463 (1997).
- 5) T. Sugino, S. Kawasaki, K. Tanioka, and J. Shirafuji, *Appl. Phys. Lett.* **71**, 2704 (1997).
- 6) Y. Kobayashi, C. L. Tsai, and T. Akasak, *Phys. Status Solidi C* **7**, 1906 (2010).
- 7) B. Arnaud, S. Lebe'gue, P. Rabiller, and M. Alouani, *Phys. Rev. Lett.* **96**, 026402 (2006).
- 8) L. Artús, M. Feneberg, C. Attacalite, J. H. Edgar, J. Li, R. Goldhahn, and R. Cuscó, *Adv. Photonics Res.* **2**, 2000101 (2021).
- 9) G. Cassabois, P. Valvin, and B. Gil, *Nat. Photonics* **10**, 262 (2016).
- 10) X. K. Cao, B. Clubine, J. H. Edgar, J. Y. Lin, and H. X. Jiang, *Appl. Phys. Lett.* **103**, 191106 (2013).
- 11) X. Z. Du, J. Li, J. Y. Lin, and H. X. Jiang, *Appl. Phys. Lett.* **106**, 021110.X. Z. Du, J. Li, J. Y. Lin, and H. X. Jiang, *Appl. Phys. Lett.* **108**, 052106 (2016).
- 12) L. Musier et al., *Phys. Status Solidi* **5**, 214 (2011).
- 13) T. C. Doan, J. Li, J. Y. Lin, and H. X. Jiang, *Appl. Phys. Lett.* **109**, 122101 (2016).
- 14) S. J. Grenadier, A. Maity, J. Li, J. Y. Lin, and H. X. Jiang, *Appl. Phys. Lett.* **112**, 162103 (2018).
- 15) A. Maity, T. C. Doan, J. Li, J. Y. Lin, and H. X. Jiang, *Appl. Phys. Lett.* **109**, 072101.A. Maity, T. C. Doan, J. Li, J. Y. Lin, and H. X. Jiang, *Appl. Phys. Lett.* **111**, 033507 (2017).A. Maity, T. C. Doan, J. Li, J. Y. Lin, and H. X. Jiang, *Appl. Phys. Lett.* **114**, 222102 (2019).
- 16) A. Maity, S. J. Grenadier, J. Li, J. Y. Lin, and H. X. Jiang, *Appl. Phys. Lett.* **116**, 142102 (2020).
- 17) J. Li, A. Maity, S. J. Grenadier, J. Y. Lin, and H. X. Jiang, *Appl. Phys. Lett.* **118**, 092102 (2021).
- 18) A. Many, *J. Phys. Chem. Solids* **26**, 575 (1965).
- 19) L. Weston, D. Wickramaratne, M. Mackoit, A. Alkauskas, and C. G. Van de Walle, *Phys. Rev.* **B97**, 214104 (2018).
- 20) S. J. Grenadier, A. Maity, J. Li, J. Y. Lin, and H. X. Jiang, "Electrical transport properties of hexagonal boron nitride epilayers," *Ultrawide Bandgap Semiconductors*, ed. Y. Zhao, (Elsevier, Amsterdam, 2021) vol 107, Chap. 12.
- 21) T. M. Al tahtamouni, J. Y. Lin, and H. X. Jiang, *J. Appl. Phys.* **113**, 123501 (2013).
- 22) P. Chan, S. P. DenBaars, and S. Nakamura, *Appl. Phys. Lett.* **119**, 131106 (2021).
- 23) X. Yang, S. Nitta, M. Pristovsek, Y. Liu, Y. Liao, M. Kushimoto, Y. Honda, and H. Amano, *2D Mater.* **7**, 015004 (2020).